Available online at www.sciencedirect.com

ScienceDirect

journal homepage: www.elsevier.com/locate/he

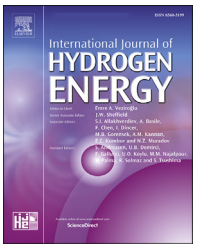

Excess heat evolution from nanocomposite samples under exposure to hydrogen isotope gases

Akira Kitamura [a,e,*], *Akito Takahashi* [a], *Koh Takahashi* [a], *Reiko Seto* [a], *Takeshi Hatano* [a], *Yasuhiro Iwamura* [b], *Takehiko Itoh* [b], *Jirohta Kasagi* [b], *Masanori Nakamura* [c], *Masanobu Uchimura* [c], *Hidekazu Takahashi* [c], *Shunsuke Sumitomo* [c], *Tatsumi Hioki* [d], *Tomoyoshi Motohiro* [d], *Yuichi Furuyama* [e], *Masahiro Kishida* [f], *Hideki Matsune* [f]

[a] *Technova Inc., Uchisaiwaicho 1-1-1, Chiyodaku, Tokyo, 100-0011, Japan*
[b] *Research Center for Electron Photon Science, Tohoku University, 982-0826, Japan*
[c] *Research Division, Nissan Motor Co., Ltd., 237-8523, Japan*
[d] *Green Mobility Research Institute, Institutes of Innovation for Future Society, Nagoya University, 464-8603, Japan*
[e] *Graduate School of Maritime Sciences, Kobe University, 658-0022, Japan*
[f] *Graduate School of Engineering, Kyushu University, 819-0395, Japan*

ARTICLE INFO

Article history:
Received 22 March 2018
Received in revised form
23 June 2018
Accepted 29 June 2018
Available online 24 July 2018

Keywords:
D_2-gas
H_2–gas
Palladium-nickel
Nanocomposite
Excess
Heat

ABSTRACT

Anomalous heat effect by interaction of hydrogen isotope gas and metal nanocomposites supported by zirconia or by silica has been examined. Observed absorption and heat evolution at RT were not too large to be explained by some chemical processes. At elevated temperatures of 200–300 °C, most samples with binary metal nanocomposites produced excess power of 3–24 W lasting for up to several weeks. The excess power was observed not only in the D-Pd·Ni system but also in the H–Pd·Ni system and H–Cu·Ni system, while single-element nanoparticle samples produced no excess power. The Pd/Ni ratio is one of the keys to increase the excess power. The maximum phase-averaged excess heat energy exceeded 270 keV/D, and the integrated excess heat energy reached 100 MJ/mol-M or 90 MJ/mol-H. It is impossible to attribute the excess heat energy to any chemical reaction; it is possibly due to radiation-free nuclear process.

Introduction

There have been continuing interests in research on various effects by hydrogen-gas charging of transition metal compounds, for application to energy storage devices and catalyser materials, and so on. The interest increased further, when palladium was used as a cathode of heavy water electrolysis to charge with hydrogen isotopes and induce extraordinarily large energy, the so-called cold fusion,

Glossary: AHE, (anomalous heat effect); MHE, (Metal-Hydrogen Energy); RT, (room temperature); ET, (elevated temperature); RC, (reaction chamber); ST, (storage tube); RTD, (resistive temperature detector); TC, (thermocouple); MPS, (mesoporous silica); FRM, (flow-rate-meter); LOCA, (loss-of-coolant accident).

* *Corresponding author*. Graduate School of Maritime Sciences, Kobe University, 658-0022, Japan.
E-mail address: kitamuraakira3@gmail.com (A. Kitamura).

https://doi.org/10.1016/j.ijhydene.2018.06.187
0360-3199/

claimed by Fleischmann-Pons in 1989. The phenomena are considered to be induced by some anomalous reactions continuing for more than weeks with reaction energies larger than chemical reactions by more than several orders of magnitude. Since then a number of experiments have been performed to reproduce the phenomenon, namely the anomalous heat effect (AHE), with use of palladium. However, most of them have been unsuccessful in replication. Only a few experiments claimed positive results using the electrolysis method or the gas-phase charging method.

Recently, nickel-based nanocomposite samples have come to gather attention owing to higher availability of nickel than palladium. A Ni·Cu·Mn alloy thin wire, for example, has been examined extensively by Celani et al. [1]. In addition, a number of entrepreneurs are publicizing their own "products" of nanofabricated samples on web sites with undisclosed details, and therefore with little scientific corroboration [*e.g.* Refs. [2,3]]. Among them, replication experiments of the Rossi-type reactors have been performed by several researchers [4–7], which seemingly appears to show unignorable reproducibility of the Rossi method. However, little is known about the accuracy of the calorimetry and the mechanism of the claimed anomalously large energy production.

On the basis of the 8 year-long (2008–2015) series of study on the AHE by interaction of metal nanoparticles and D(H)-gas under the collaboration of Technova Inc. and Kobe University, a collaborative research project has begun aiming at scope of industrial application to a new CO_2-free, distributed energy source [8]. Based on the Technova-Kobe works, new project on MHE (Metal-Hydrogen Energy) was started on October 2015 under the collaboration of six Japanese organizations, one of which the individual author of the present paper belongs to. The results of the early-stage research program were reported in 20th International Conference on Condensed Matter Nuclear Science (ICCF20) [9,10], 17th Meeting of Japan CF-research Society (JCF17) [11,12] and 12th International Workshop on Anomalies in Hydrogen Loaded Metals [13,14].

In the present paper, we report results of observation of AHE by interaction of hydrogen isotope gas and nanocomposite samples done as the collaborative work using the experimental apparatus installed at Kobe University [15–18].

The system has a reaction chamber containing the sample with a capacity of 500 cc, and an oil-flow-calorimetry system capable of working at elevated temperature (ET) up to about 350 °C with use of a synthetic liquid hydrocarbon coolant, Barreltherm-400 (BT400). The samples tested so far as the collaborative work include both zirconia-supported and silica-supported metal nanoparticles. In the present paper, hydrogen isotope (D or H) absorption and heat-generation characteristics of the samples are discussed with emphasis on those under rather constant pressure condition after initial D(H)-absorption process or even during effectively net desorption process at elevated temperature.

Experimental procedure and samples

A schematic of the D(H)-gas-charging-calorimetry system C_1 is shown in Fig. 1. The reaction chamber (RC) containing the sample has two kinds of electric heaters to elevate the temperature of the sample; one wounded around the RC capable of giving the power (W_1) of up to 1 kW, and the other inside the RC through the bottom flange giving the power (W_2) up to

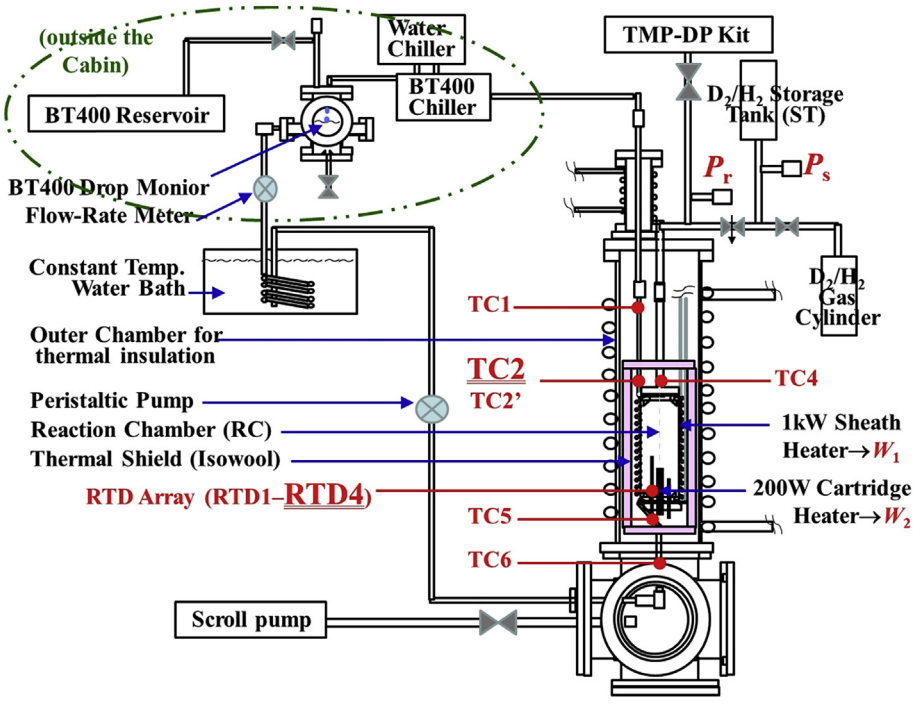

Fig. 1 – Schematic of C_1 MHE-experimental system equipped with oil-flow-calorimetry system with flow-rate-monitors and dual heaters mounted on the reaction chamber (RC).

200 W. A stainless steel pipe for the coolant BT400 is wound in parallel with the W_1 heater.

Four resistive temperature detectors (RTD1 ~ RTD4) are inserted into the RC to measure directly the temperature of the sample with the sensitive points at 3, 6, 9 and 12 cm from the bottom. To measure the coolant temperature and calculate the heat flow rate, six K-type thermocouples, TC1 through TC6, are attached on the coolant pipe as shown in the figure. The third one is located at the same vertical position with TC2 to check the reliability, and called TC2'. The heat flow rate is calculated from difference in temperatures at TC2 and TC6, (T_{C2}-T_{C6}), and the flow rate of BT400, R_f.

Hydrogen isotope gas, D_2 or H_2, is fed from the storage tube (ST) through a needle valve. The amount of D(H) absorbed by the sample, or the apparent loading ratio $L_M \equiv$ (D/M) or (H/M), is calculated as the number of hydrogen isotope atoms lost from the gas phase relative to the number of metal atoms (Pd(Cu) and Ni in PNZ (CNZ) runs). It is calculated from the pressures at the RC and the ST, P_r and P_s, respectively, and their volumes with a correction for the temperature based on the Boyle-Charles' law with use of the averaged temperature of four RTD's.

The RC is located inside an outer chamber evacuated for the purpose of thermal insulation, and covered with a dewar-like ceramic-fiber casing to reduce the radiation loss. The coolant BT400 heated at the RC is circulated with a peristaltic pump, and cooled with a chiller located outside the cabin which is air-conditioned at a constant temperature within a variation of ±0.1 °C. The coolant temperature is further regulated inside the cabin with a temperature-controlled water bath keeping usually 25 °C with a variation less than ±0.1 °C. The flow rate of the coolant is monitored with two flow sensors with elliptic gears; one for the logger signal, and the other for cross-checking.

The sample name is composed of the initial letters of the atomic symbol of the constituent elements followed by a number indicating the production order, which may be further followed by either "r" for re-calcined sample, "f" or "n" for the sample fabricated in Kyushuu Univ. (Fukuoka) or in Nagoya Univ. (Nagoya), respectively. The samples from the same lot are distinguished by a letter "s" or "k" for use in Tohoku Univ. (Sendai) or Kobe Univ., respectively.

As the collaborative work, sixteen kinds of samples were tested; ZrO_2-supported binary nanoparticle samples (Z-type; PNZ3, PNZ3f, PNZ3r, PNZ4s, PNZ5, PNZ6, PNZ7k, CNZ5, CNZ5s, CNZ6s and CNZ7s), SiO_2-supported binary nanoparticle samples (S-type; CNS3 and CNS3s), and SiO_2-supported single-element nanoparticle samples (S1-type; PS3, PSf1 and PSn1). Among them nine samples (PS3, PSf1, PNZ3, PNZ3r, PNZ5, PNZ6, PNZ7k, CNZ5 and CNS3) were tested in Kobe Univ., while in Tohoku Univ. six samples (PSn1, PNZ4s, CNZ5s, CNZ6s, CNZ7s and CNS3s) were tested with use of a system with similar specifications to those in Kobe Univ. One sample (PNZ3f) was tested in Kyushu Univ. with use of the commercial DSC apparatus capable of measuring small amount of the sample of the order of mg precisely. Reports of results of the tests at Tohoku University and Kyushu University will be published elsewhere.

Besides, three samples (PNZ4, PNZ5r and PNZ6r) were tested as independent experiments in the collaborative research period in Kobe Univ. In addition, one sample (PNZ9) and eleven samples (PNZ8A ~ E, CNZ8A ~ D and CNZ9A ~ B) fabricated by Technova Inc., were tested in Tohoku Univ. and Kyushu Univ., respectively.

The Z-type samples were prepared by the melt-spinning method similar to that used in Ref. [19]. The alloy-compounds of $Pd_xNi_{0.35-x}Zr_{0.65}$, *e.g.*, were prepared by arc-melting of the component metal blocks. The alloys were melted again by RF heating, and rapidly solidified with a melt-spinning machine to make ribbon-like thin sheets of amorphous $Pd_xNi_{0.35-x}Zr_{0.65}$ compounds. The thin sheets were calcined in air at a temperature of 450 °C for 60 h, during which preferential formation of ZrO_2 supporter zone with isolated distribution of nano-structure zones of $Pd_xNi_{0.35-x}$ is expected. They were then ground in a mortar to make the sample particles with diameter of several to tens of μm. The composition parameter x is 0.044 (Pd/Ni = 1/7) for most samples tested in Kobe Univ [9,13,15,18]. including the CNZ-type with Cu/Ni = 1/7, except for PNZ6 and PNZ6r with $x = 0.032$ (Pd/Ni = 1/10). It will be found that the composition parameter x is one of the most important variables for excess power production. The oxygen content was evaluated from the weight difference before and after the calcination/re-calcination. Only about 5%–10% of 500-cc volume of the RC was occupied by 100–200 g of the Z-type sample itself, and the rest 95%–90% was filled with 1-mm-diameter zirconia beads (ZrO_2 filler) for the AHE measurement.

The S-type samples are $CuNi_y$ nanocomposites supported by mesoporous silica (MPS), PC700G, Admatechs Co. Ltd. The samples were synthesized in Kobe Univ.; the MPS powder was put into the aqueous ammonia solution dissolving $CuCl_2$ and $NiCl_2$ with molar ratio of 1:7. After stirring and suction filtration, the samples were calcined at 800 °C for 3h to obtain the MPS with the nanocomposites adsorbed on the mesoscopic pore surface and/or the outer surface of the MPS particles. A STEM/EDS analysis showed that the size of the $CuNi_y$ nanocomposites ranged from several to several tens of nm.

The PSf1 sample fabricated in Kyushu Univ. is about 3-nm diam. Pd nanoparticles embedded in 10-nm-thick SiO_2 microparticles, while the PSn1 sample fabricated in Nagoya Univ. is size-controlled Pd nanoparticles with the average diameter of 3.9 nm supported by mesoporous silica, TMPS4R, Taiyo Kagaku Co. Ltd. Both the S1-type and the S-type samples occupied the RC without any filler.

ICP-AES and XRD analyses for some Z-type samples, PNZ3, PNZ3r, PNZ4, PNZ5 and CNZ5, were done at Nissan Motor Co. Ltd., Kyushu Univ., and Nagoya Univ. independently. A lot of interesting features including evolution of crystalline phases of $NiZr_2$, ZrO_2, etc., have been revealed, which will be published independently elsewhere.

STEM/EDS analyses for PNZ3, PNZ3r, PNZ4 and CNZ5 samples done at Kobe Univ. showed interesting features of nanostructure of the Z-type samples: (1) Most Pd(Cu) and Ni atoms are found in the same areas. (2) After absorption runs, $NiZr_2$ decreased, and ZrO_2 increased. (3) After re-calcination, the apparent majority became ZrO_2 + NiO + Pd(Cu)O [8,18]. Other STEM/EDS analyses performed by Nissan Moter Co. Ltd. revealed unexpected structure of the oxide layers, which will also be published independently elsewhere.

For the samples discussed in the present paper in detail, PNZ6, PNZ6r and PNZ7k, neither XRD, ICP-AES nor STEM/EDS was performed. However, there is no reason to assume characteristics different from PNZ3, PNZ3r, PNZ4 and PNZ5 samples for formation of nano-structure.

Calibration of the flow calorimetry was performed with use of a dummy sample, pure zirconia beads for ZrO_2-supported samples. The heat conversion coefficient from the power to the temperature difference, d $(T_{C2}$-$T_{C6})/dW \approx dT_{C2}/dW$, was obtained; *e.g.*, 1.57 °C/W at room temperature (RT) or 1.0 °C/W at about 300 °C in the RC for the flow rate of 20 cc/min. The heat recovery rate, $R_h = 0.88–0.83$ in the temperature range from RT to 300 °C, was calculated by

$$R_h = R_f{}^{\alpha} \cdot \rho \cdot C \cdot (T_{C2} - T_{C6})/(W_1 + W_2), \quad (1)$$

where R_f, ρ and C are the flow rate, the mass density and the specific heat capacity, respectively, of the coolant BT400. The parameter α was determined empirically as follows. A correction factor for the flow rate fluctuation ΔR_f $(= R_f – R_{f0})$ to be subtracted from T_{C2} is derived from eq. (1);

$$\Delta T_{C2} = (dT_{C2}/dR_f) \cdot \Delta R_f = (-\Delta R_f/R_f) \cdot (W_1 + W_2) \cdot (dT_{C2}/dW) \cdot \alpha. \quad (2)$$

The correction is applied to T_{C2} for some samples or gas species to determine α, so that the corrected temperature is not unreasonable, not giving negative excess temperature, or giving null excess for the Ar filling run, in the flow rate range of $0.825 \le R_f/R_{f0} \le 1$ for $R_{f0} = 20$ cc/min;

$$\alpha = 1.9 \times 10^{-2} \cdot \exp[4.0 \cdot (R_f/R_{f0})]. \quad (3)$$

The calibration run serves also as a control run giving reference values of the temperatures, the flow rate of BT400 and the heater power for foreground runs using the ZrO_2-supported samples with the pure zirconia beads filler. Comparing the temperatures in the foreground and background runs, the excess power will be calculated using the heat conversion coefficient mentioned above.

For SiO_2-supported samples, the calibration was similarly done with use of bare silica powder to obtain the heat recovery rate, $dT_{C2}/dW = 1.65$ °C/W or 0.95 °C/W, and heat recovery rate, $R_h = 0.88–0.79$, in the same temperature range as above for ZrO_2-supported samples. The calibration run serves as a control run for foreground runs using the SiO_2-supported samples with no filler.

Usual procedure of the absorption/heat-evolution measurement is as follows. Hydrogen isotope gas initially 1 to 0.7 MPa at the ST is introduced into the RC initially vacuum at RT containing a virgin sample after vacuum baking/outgassing at a temperature above 200 °C. After a few hours in most cases, D (or H) absorption is saturated and associated heat evolution is terminated (phase 1 of #1 run; #1-1). Then the phase #1–2 at some ET is initiated with some heater power (W_1, W_2). After reaching a quasi-steady state the heater power is varied to proceed to the next phase #1–3, and similarly to #1-m ($m = 4, 5, \ldots$). The combination of W_1 and W_2 or the power ratio is chosen to be approximately 3:2, so that the temperature distribution in the RC is as uniform as possible. At the end of the #1 run, the RC is evacuated under an ET condition to degas the sample, namely the baking process.

For the nonvirgin sample which experienced the above processes, the series of the procedure from D(H) introduction at RT to evacuation at ET is repeated to obtain a series of data set for #2-m ($m = 1, 2, 3, \ldots$) phases. Since metal elements in the virgin sample are usually oxidized to some extent, and reduced by D(H) introduction, one of the reasons for difference in the absorption and heat evolution data between #1 and #2 or later, if any, could be the existence of the oxidized metal atoms in #1 runs presumably.

Results and discussion

PNZ samples

Most experiments done at Kobe Univ. as the collaborative examinations used Z-type samples. Among them the PNZ samples (PNZ3, PNZ4, PNZ5, PNZ6 and PNZ7k) except for re-calcined ones (****r) showed similar absorption/heat-evolution characteristics at RT, while at ET they showed different excess power. The characteristics are explained below with PNZ6, PNZ6r and PNZ7 taken as examples.

D(H) absorption

Deuterium (D) or protium (H) absorption runs, PNZ6#1, #2, #3 and #4, were performed after vacuum baking (#0) for more than 30 h at RTD and TC2 temperatures of 200–300 °C with the heater power of $(W_1+W_2) = (69 + 20) \sim (124 + 30)$ W and with the nominal BT400 flow rate of 20 cc/min. The temperature history in the D-PNZ6#0 through #4 is shown in Fig. 2. Each time the heater power was varied, the phase number was advanced, as mentioned above. At the end of each run the heated sample was degassed by evacuating the RC, and the run number is advanced for the succeeding run started with filling of the fresh D_2 or H_2 gas.

In the figure also shown is the variation of the flow rate R_f of BT400. Although R_f has rather large fluctuation of ~10%, the temperature variation due to the fluctuation of R_f is properly corrected for by Eq. (2). In the #1 run, there was a trip of the flow-rate-meter (FRM). Then it was replaced with new one. Another trouble we encountered twice was the loss-of-coolant accident (LOCA) at #2-2′ and #2–3′ phases. In spite of these troubles, we observed rather stable temperature evolution giving large excess power.

The pressures at the RC and at the ST, P_r and P_s, respectively, and the apparent loading ratio $L_M \equiv$ (D/M) or (H/M) are shown in Fig. 3. It should be noted that the apparent loading ratio L_M reaching 3.5 was exceptionally large in the #1-1 RT phase. It decreased to below 3.0 due to desorption under elevated temperature in #1–2. Then it increased gradually due to unexpected leakage of D_2 gas from the RC. The relatively large leakage continued until it was partly fixed at the end of the #2–3′ phase, after which the leakage became much smaller. However, the leakage has little influence on L_M in the RT phases, #n-1 ($n = 1–4$).

The variation of L_M with the leakage component subtracted is briefly discussed below. The sample after #0 baking is assumed to be composed of ZrO_2, $NiZr_2$, NiO and PdO based on the XRD measurements. The possible sources of D

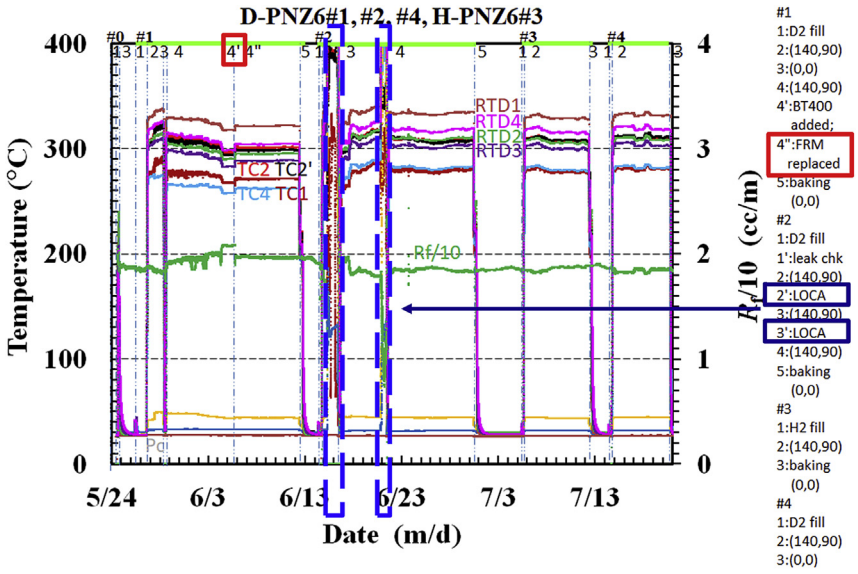

Fig. 2 – Evolution of temperature and oil flow rate R_f in PNZ6#0 through #4 runs.

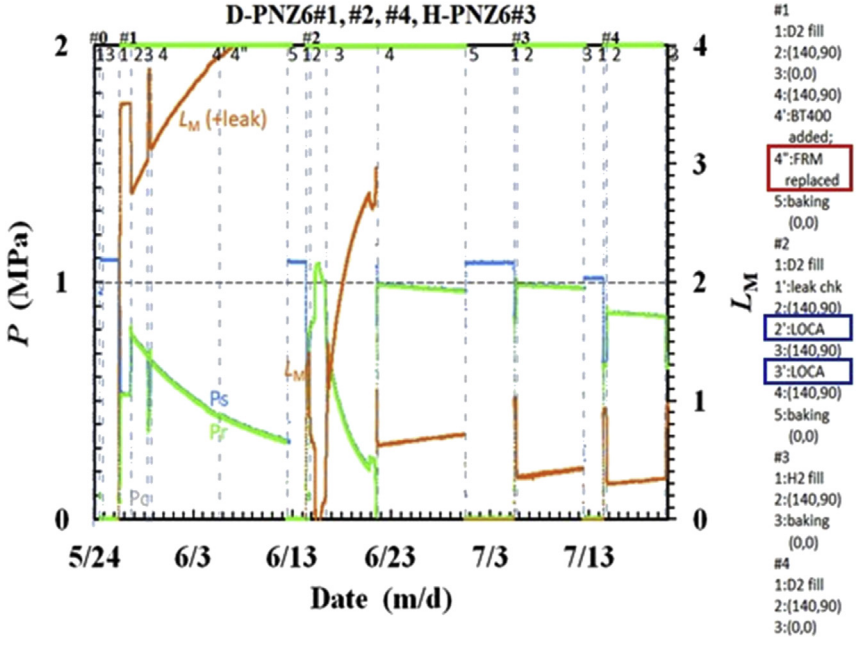

Fig. 3 – Evolution of hydrogen loading ratio L_M (=D/M) and D(H)-gas pressure in PNZ6#1~#4 runs.

consumption are reduction of oxides, reactions (4) and (5) below, absorption by Pd and Ni, (6) and (7), and absorption by $NiZr_2$, (8);

$$PdO + D_2 \rightarrow Pd + D_2O + 1.77eV/Pd, \quad (4)$$

$$NiO + D_2 \rightarrow Ni + D_2O + 0.177eV/Ni, \quad (L_M = 2.0) \quad (5)$$

$$Pd + (a/2)D_2 \rightarrow PdD_a + 0.2eV/Pd, \quad (L_M = a) \quad (6)$$

$$Ni + (b/2)D_2 \rightarrow NiD_b + (0.1 \sim 0.2)eV/Ni, \quad (L_M = b) \quad (7)$$

$$NiZr_2 + (c/2)D_2 \rightarrow NiZr_2D_c + E_{NiZr2} \quad (L_M = c) \quad (8)$$

In ET phases #1-n ($n \geq 2$), desorption of D (reversed (6), (7) and (8)) would proceed, which makes L_M decrease.

At the end of the #1 run the sample was degassed by evacuating the RC at ET. By this procedure the gases produced by the reactions, D_2O ((4), (5)) and D_2 ((6), (7), (8)) are removed from the system. Then the sample composition after the #1 baking is thought to be ZrO_2, $NiZr_2$, $NiZr_2D_c$, and reduced metals (Ni + Pd). Here it is assumed that $NiZr_2D_c$ and $PdD_a \cdot NiD_b$ lose D partially during desorption under ET; only a part of $NiZr_2D_c$ turns back to $NiZr_2$ and/or $NiZr_2D_{c'}$ ($c' < c$), and similarly for $PdD_a \cdot NiD_b$. This together with the absence of the oxides would be one of the possible reasons why the D

consumption in the #2-1 phase drastically decreased compared with that in the #1-1.

It is well known that pure Ni cannot absorb H isotopes at RT. If we exclude Ni from "M" used in the calculation of L_M, we have impossibly large L_M, one order of magnitude greater than those shown in Fig. 5. Then we conclude that a small amount of Pd is working as a catalyser for H isotope absorption of Ni at RT.

Heat evolution at RT

The initial bursts of heat are observed on the RTD and TC traces at the beginning of the #1-1 phase at RT. Fig. 4 shows the thermal power calculated from the temperature evolution in the #1-1 phase with use of the conversion factor mentioned above. The heat evolution has two peaks, simply because fresh D_2 gas was resupplied to the ST at 3.9 h after the initial introduction of D_2 gas. By the resupply the pressure of D_2 in the ST and therefore the flow rate of D_2 was increased to enhance the rate of heat evolution associated with absorption of D_2.

The hump at TC2 is time-integrated to calculate the total emerging energy per an absorbent atom,

$$E_a = \int_0^t W_a dt, \tag{9}$$

where W_a is the power per an absorbent metal atom M, *i.e.*, both Pd and Ni in the present case of the PNZ sample. The total energy E_a is calculated to be 1.9 ± 0.1 eV/M. This is rather large in view of the hydrogen absorption energy of about 0.2 eV/Pd for bulk crystalline Pd. The energy E_a is divided by L_M to obtain the specific "absorption" energy, the averaged energy in the relevant phase per D atom adsorbed/absorbed or lost from the gas phase, $\eta \equiv E_a/L_M = (5.8 \pm 0.3) \times 10^{-1}$ eV/D. Similarly, E_a and η are calculated for #*n*-1, where *n* is the integer representing the run number. Those together with L_M are summarized in Fig. 5, and compared with those of PNZ6r and PNZ7k samples.

Some conclusions are deduced from the figure. First of all, PNZ7k is similar to PNZ6 in regard to these quantities. The reproducibility is rather good in spite of the difference in Pd/Ni.

Secondly, we notice the exceptionally large value of L_M at #1-1, and gradual decrease of L_M in the following phases. The difference between L_M in #1-1 and that in #2-1 is almost 2. As has been partly discussed in the preceding subsection, possible reasons for this large difference are the following. (1) In the ET phases only a part of $NiZr_2D_c$ liberate D_2 turning back to $NiZr_2$ or $NiZr_2D_{c'}$ ($c' < c$). The liberated D_2 gas is removed by evacuation at the end of the #1 run. (2) Similarly, only a part of $PdD_a{\cdot}NiD_b$ could liberate D_2 turning back to $PdD_{a'}{\cdot}NiD_{b'}$. (3) The oxides PdO·NiO to be deduced to metallic Pd·Ni by consuming D_2 is absent or very few in the #2 run. As for the isotope effect on L_M, it appears that the difference between D-charging and H-charging is too small to be distinguished from the change in sample properties as discussed above.

Third, the specific absorption energy per D atom, η, have essentially the same value (0.3–0.4 eV/D) in PNZ6#*n*-1, where $n \geq 2$. This infers that the underlying physics is the same in the PNZ6#*n*-1 phases. In other words, this means that the reduction of PdO·NiO, if any, was almost completed in #1-1, and that the values of η in #*n*-1 ($n \geq 2$) are the intrinsic ones for the sample. Possible processes responsible for this are the deuterium absorption by Pd·Ni, the reactions (6) and (7), and by $NiZr_2$, the reaction (8). Gradual decrease of L_M and E_a suggests that decomposition of $NiZr_2$ and/or some structural degradation of the Pd·Ni nanostructure are proceeding. The intrinsic η ~0.4 eV/D is larger than that for the bulk Pd (~0.2 eV/D). Possible reasons for this are the following; (1) The absorption energy E_{NiZr2} in the reaction (8) is rather large. (2) It might be possible that the absorption energies in the reactions (6) and (7) become larger, when Pd and Ni form nanocomposites. (3) It might also be possible that some unknown reactions other than absorption occur in the Pd·Ni

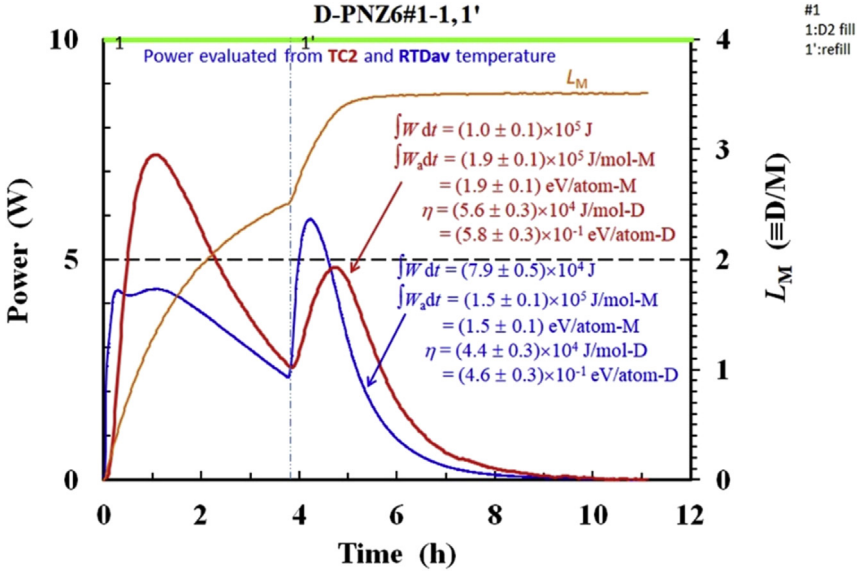

Fig. 4 – Thermal power and deuterium loading ratio in the RT phase of the virgin sample run, D-PNZ6#1-1.

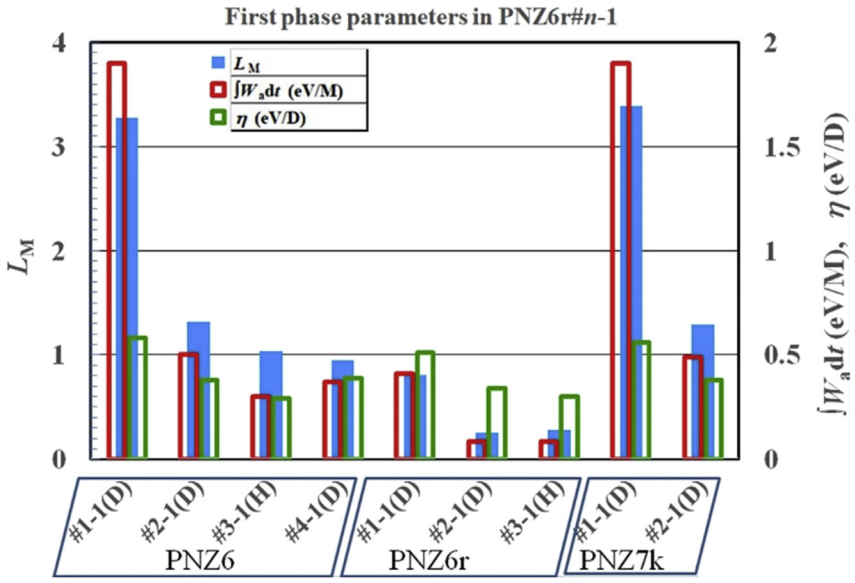

Fig. 5 – Comparison of loading ratio and specific absorption energies in RT phases of PNZ6#1-1 through PNZ7k#2-1 runs.

nanocomposites. In #1–3 with the filling gas of H_2, η is decreased by about 25% possibly due to the isotope effect. Anyway, it is difficult to discuss these points further before knowing the composition quantitatively.

Fourth, the PNZ6r runs have similar variation of L_M and E_a but with smaller amplitude. It appears that this is because the numbers of the absorbers, $NiZr_2$ and NiO, are reduced in comparison with the PNZ6. It seems that, by re-calcination, some fraction of $NiZr_2$ are likely to be decomposed to ZiO_2 and Ni/NiO, and some fraction of Pd·Ni nanostructure might be changed to different one relatively inactive in regard to absorption.

Heat evolution at ET

Next, we discuss the oil-outlet temperature T_{C2} in the ET phases in the PNZ6 runs, T_{C2} (the red line in Fig. 6), in comparison with $T_{C2}(ZrO_2)$ in the calibration/control run using the zirconia beads (the black line in Fig. 6). As is shown, T_{C2} is higher than $T_{C2}(ZrO_2)$ in most ET phases. When we take into account the fluctuation of the heater power and the flow rate as seen in Fig. 2, and apply the correction according to Eq. (2), we obtain the curve shown as the green line in Fig. 6.

The difference is converted to excess power, W_{ex}, by dividing it by dT_{C2}/dW, and shown in Fig. 7. The excess power of 10–24 W is rather large. When we take into account the systematic error of ±2.3 W determined from fluctuations recorded in blank runs and S1-type sample runs (described later), the maximum excess power is more than one order of magnitude higher than the error range. In the PNZ6 sample powder some anomalous effect is induced to generate the excess power in all phases with the elevated temperature of 300–340 °C at RTD1 ~ RTD4. There could be an isotope effect on the excess power. However, the difference is too small to be distinguished from fluctuation of the excess power.

The phase-averaged excess heat energy, $\eta_{av,i}$ (closed circles), and the integrated excess energy per an absorbent atom, E_a (integrated W_{ex} per absorbent atom; closed squares), in the elevated temperature phases are also plotted in Fig. 7. It should be noted that $\eta_{av,i}$ is defined as E_a divided by the absolute value of ΔL_M, the increment of adsorbed/absorbed or desorbed deuterium atoms, both in the relevant phase i;

$$\eta_{av;i} \equiv \frac{\int_0^{T_i} W_a dt}{|\Delta L_M(T_i)|}, \tag{10}$$

The absolute value is taken to keep $\eta_{av,i}$ positive under desorption. This is because we assume that the exothermic event could occur along with hydrogen isotope displacement under both absorption and desorption. The maximum value of $\eta_{av,i}$ exceeds 10 keV/D, and the integrated excess energy E_a reaches 1 keV/M (100 MJ/mol-M).

The definition of $\eta_{av,i}$ is rather problematic, since the real number of the hydrogen atoms getting in and out of the surfaces of the nanoparticles is not always represented by $|\Delta L_M|$ in the denominator of Eq. (10). However, even if we divide E_a by the total amount of D absorbed in each run, L_M, to evaluate the integrated excess energy per a D atom participating in the absorption, the energy is still far beyond the value explainable by any chemical reaction; $E_{ex} \equiv E_a/L_M = 460$ eV/D = 44 MJ/mol-D in the D-PNZ6#4 run. Since any chemical reaction is a process of changing orbital electron configuration, the reaction energy never exceeds the binding energy of the electron, *e.g.*, 13.6 eV for hydrogen isotope. The large values of the excess energy suggest a nuclear origin of the excess heat.

It is important to note that the sudden increase of W_{ex} in the #1–2 phase is really spontaneous. Fig. 8 shows the unexpected, unintended evolution of the excess power in the #1–2 phase having no correlation with the fluctuation of the flow rate nor the input heater power. It also shows the temperatures at other TCs and RTDs during the same period of time. The unexpected, unintended evolution of the excess power appears to originate in the peripheral region of RC. This is because the step-like increases of the temperatures are

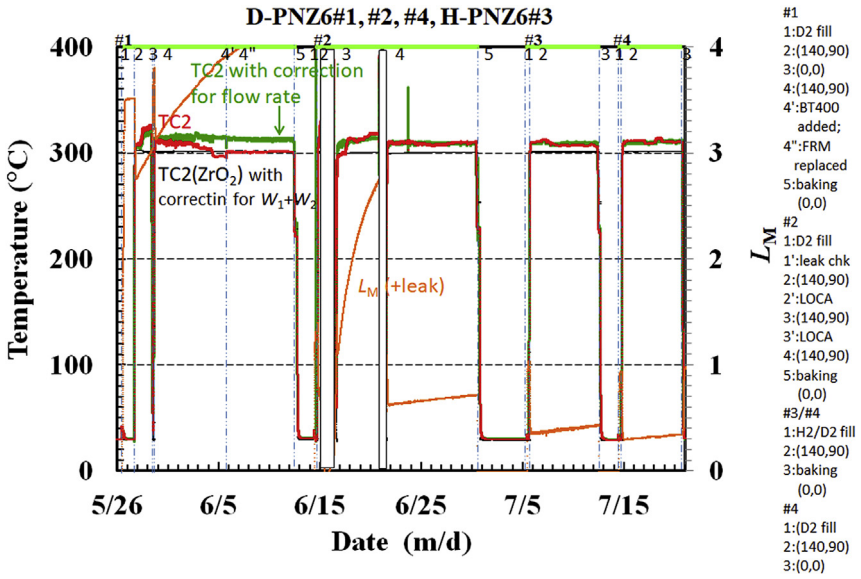

Fig. 6 – Difference in TC2 temperature between the foreground (PNZ6) run and the blank (ZeO_2 beads) run.

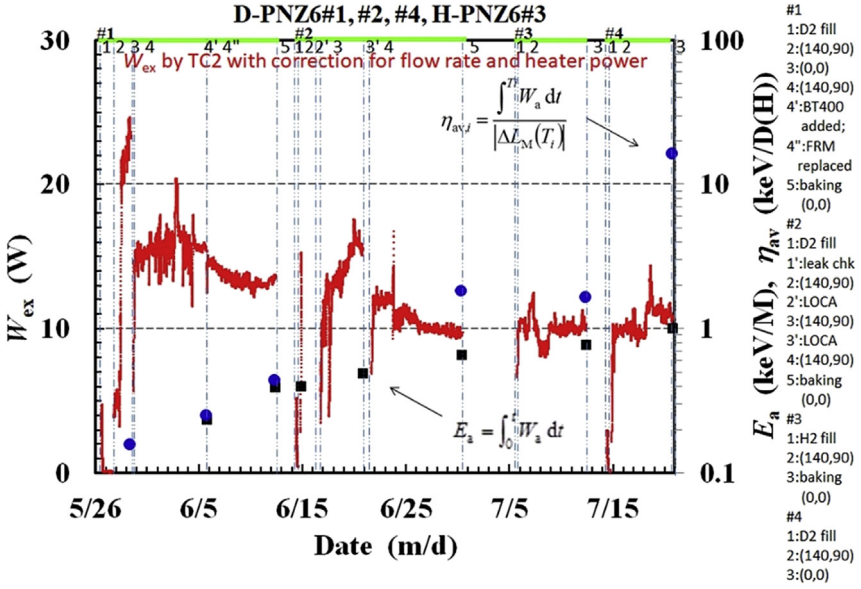

Fig. 7 – Excess power, W_{ex}, integrated excess energy per absorbent atom, E_a (keV/M), and phase-averaged excess heat energy per hydrogen isotope atom absorbed/desorbed, $\eta_{av,i}$ (keV/D(H)), in RT and ET phases evaluated by TC2 temperature.

observed with much smaller amplitude in RTDs which are relatively insensitive to the temperature at the peripheral region. The excess power in the #1–2 phase reaching 24 W is largest among all sample runs tested so far.

The PNZ6 sample was re-calcined after finishing the PNZ6#4 run. The sample is called PNZ6r, and similar sequence of heater power application was given to the PNZ6r sample. As might be supposed from L_M for the RT phases shown in Fig. 5, deuterium absorption is weaker than PNZ6; L_M in the ET phases, #1–2 through #1–5, is about 0.5 and smaller than 0.3 in #2-2 ~ 4 and #3-2 phases. However, the excess power and the excess energies are comparable to or even greater than those in PNZ6; W_{ex} is ranging from 5 to 10 W, $E_a \approx 0.53$ keV/M (55 MJ/mol-M), $\eta_{av,i}$ and E_{ex} reaching 270 keV/D and 85 MJ/mol-D, respectively. These values again make it realistic to assume a nuclear origin of the excess heat.

Fig. 9 shows peculiar evolution of temperature observed in the PNZ6r#1–2 phase. Relatively large humps are recorded in the RTD1 and RTD2 traces. The figure also shows desorption under elevated temperature in #1–2 similar to other samples, but with exceptionally large time constant. The reason for these phenomena is not known. However, it is very interesting to see that large positive excess power evolution was generated under the net desorption process. This effect seems to infer that the nuclear-like reaction sites exist in the near-surface of the $PdNi_x$ nanocomposites.

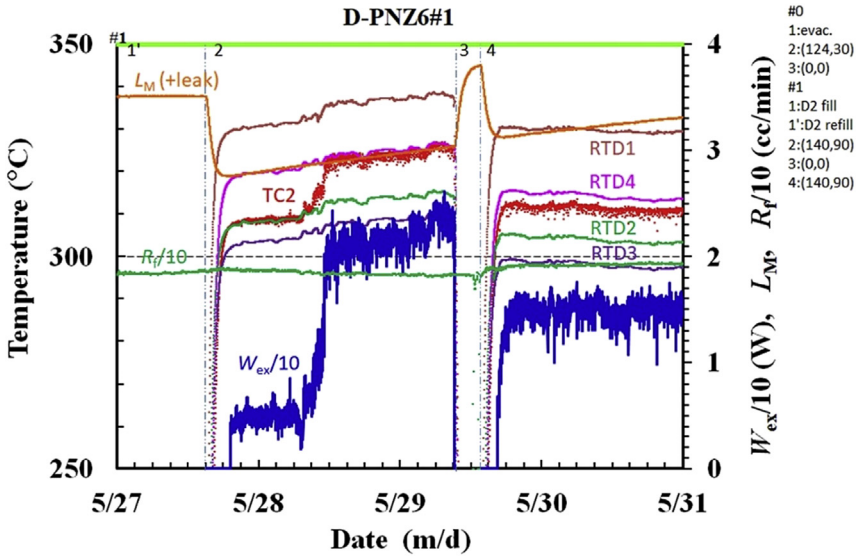

Fig. 8 – Temperatures at TC2 and at RTDs, the loading ratio L_M and the flow rate R_f, showing unexpected, unintended evolution of the excess power W_{ex}.

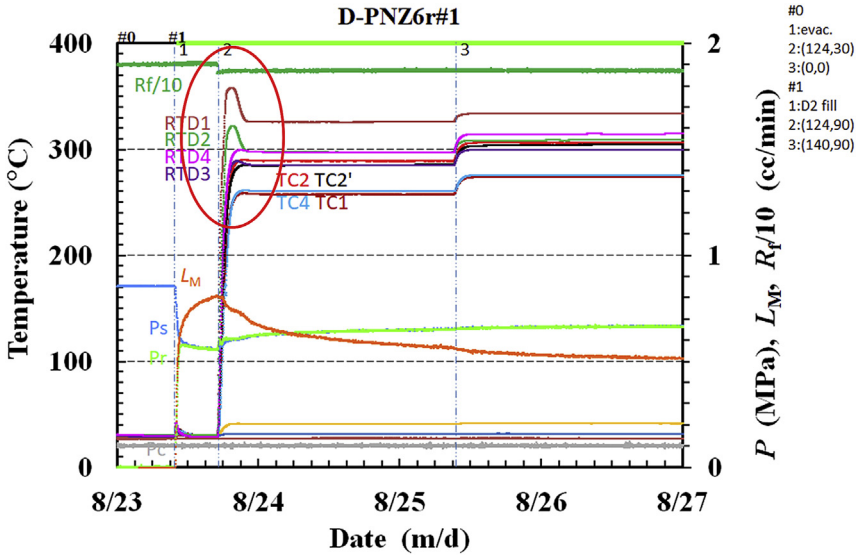

Fig. 9 – Peculiar evolution of temperature in the D-PNZ6r#1–2 phase.

A similar phenomenon of local heat evolution was observed in the D-PNZ5r#1 and #2 runs. Temperatures at RTD1 and RTD2 were higher in the #1–2 and #1–3 phases than in the control run by about 100 °C and 60 °C, respectively, while increase in the TC2 temperature was modest, giving an excess power of about 4 W. If we tentatively calculate the excess power using a temperature averaged over those at RTD1 through RTD4, we have the excess power of 30 W. In the #2-2 phase after baking at #1–4 and #2-1 RT phase, however, the tentative excess power calculated from the RTD averaged temperature gradually decreased to 12 W, while the TC2 excess power increased to about 5 W. This is an interesting phenomenon, since we know from the calibration runs that the heat conduction properties of the sample powder to the coolant has very little influence on the TC2 temperature. It is inferred that the spot of the local heat evolution moved from somewhere near the RTD1 and RTD2 to somewhere near the peripheral region.

Next, the PNZ7k sample with the atomic ratio of Pd/Ni = 1/7 is compared with PNZ6 and PNZ6r discussed above. As has been mentioned earlier, this sample in the RT phases shows characteristics very similar to those for the PNZ6 sample. The similarity is also true for L_M in the ET phases but without leakage. However, there is a large difference in excess power and energies. These are shown in Fig. 10. The excess power W_{ex} and accordingly the integrated excess energy E_a are appreciably small compared with those for PNZ6 and PNZ6r. As for the phase-averaged excess heat energy, $\eta_{av,i}$, the values

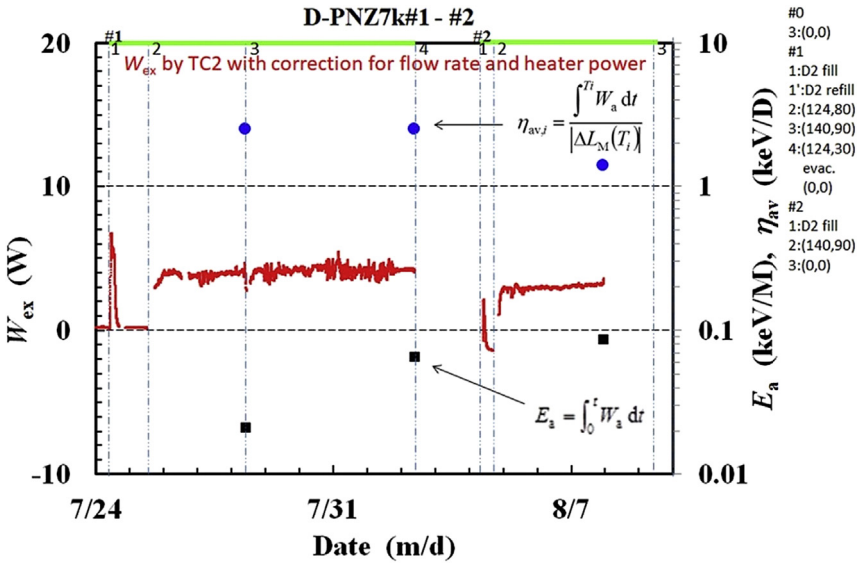

Fig. 10 – Excess power W_{ex}, integrated excess energy per metal atom E_a (keV/M) and phase-averaged excess heat energy $\eta_{av,i}$ (keV/D), in PNZ7k runs.

are not very small, yet remarkably large values are not observed. From these facts we conclude that the atomic ratio of the binary absorbent metal in the sample is one of the key factors to increase the excess power. The smaller the ratio of the minority species to the majority, the larger the excess power. However, it will be shown later that the single-element nanoparticle sample never produce the excess heat in ET phases [11]. We have to look for the most suitable atomic ratio.

CNZ sample

It was found that the CNZ-type samples after calcination have almost no XRD peaks originating in $NiZr_2$. Differently from the PNZ-type samples, preferential oxidation of Zr to ZrO_2 was completed in the calcination process, and nanocomposites of Pd·Ni and/or PdO·NiO are dispersed in the ZrO_2 crystalline phases of the virgin sample.

Variations of temperatures at TC2 and RTD1 ~ RTD4 and the loading ratio L_M in the H-CNZ5 run are shown in Fig. 11. In the #1-1 phase at RT, Cu and Ni nanocomposite particles showed rather weak absorption of H; L_M ~0.2 with a rather large η ~0.5 eV/H approximately equal to those in the PNZ runs. At ET around 200 °C, however, L_M increased up to 1.9. In addition, a localized heat evolution near RTD1 and RTD2 similar to those observed in the PNZ5r and PNZ6r runs is observed. The excess power tentatively calculated from the averaged RTD signals is about 8 W.

Unfortunately, the absorption run with the CNZ5 sample was aborted at #1–5 phase, when we recognized a welding defect on the coolant pipe that could change the heat recovery

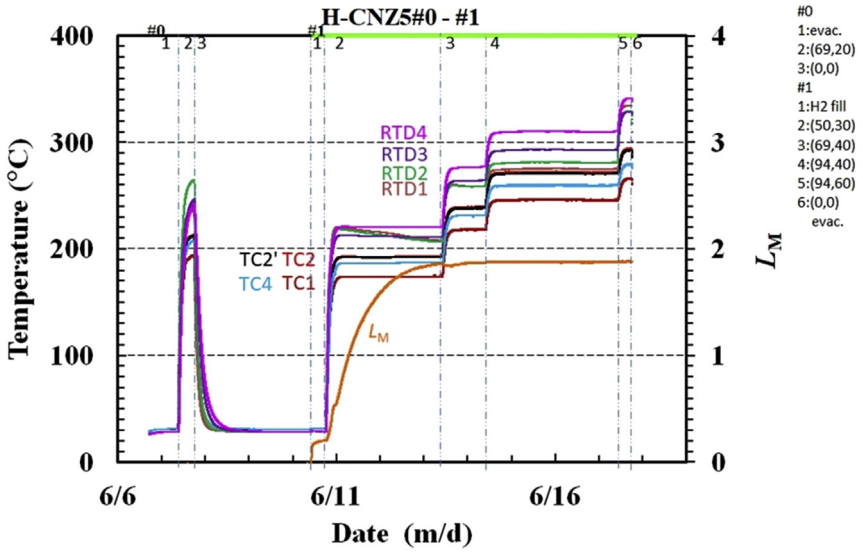

Fig. 11 – Variation of temperatures and loading ratio L_M in CNZ5 runs.

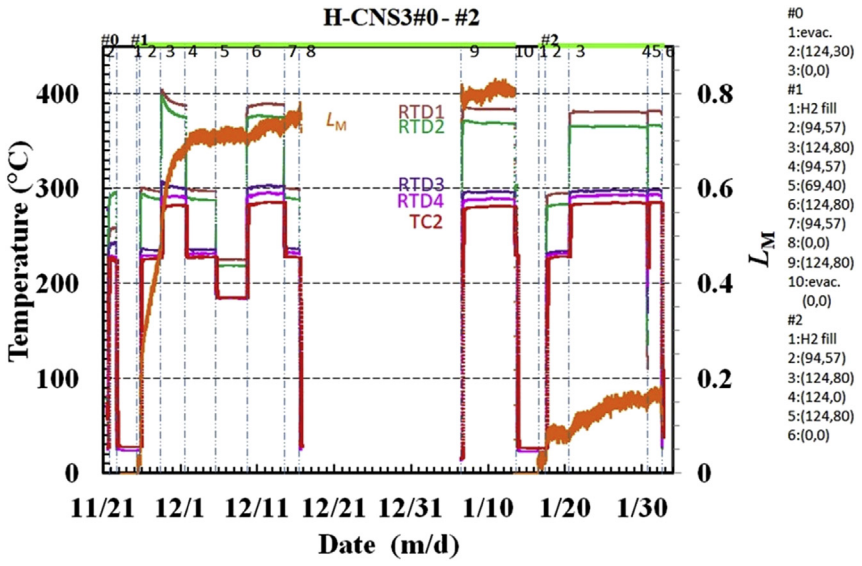

Fig. 12 – Variation of temperatures and loading ratio L_M in CNS3 runs.

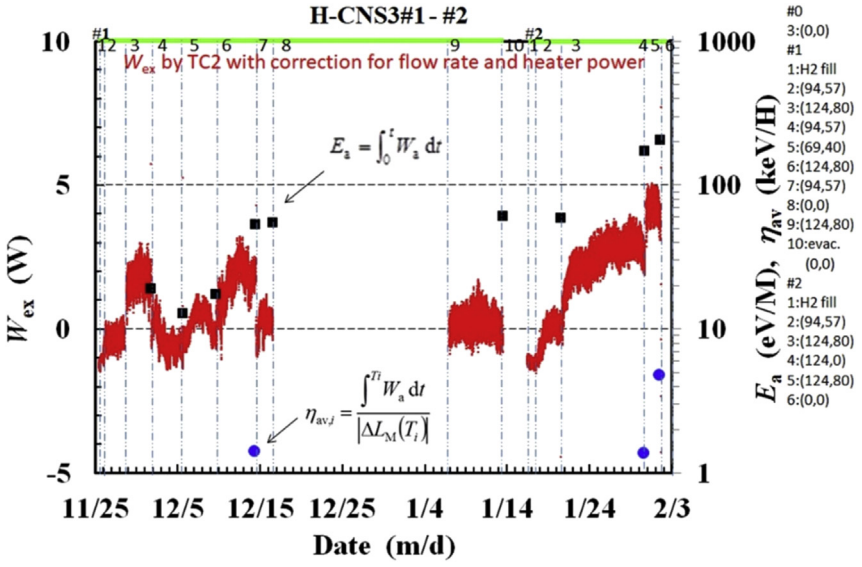

Fig. 13 – Excess power W_{ex}, integrated excess energy per metal atom E_a (keV/M) and phase-averaged excess heat energy $\eta_{av,i}$ (keV/D), in CNS3 runs.

efficiency. Other CNZ samples were tested in Tohoku Univ. which will be published independently.

CNS sample

Variations of the temperatures and L_M in the CNS3 run are shown in Fig. 12. The excess power calculated from the TC2 temperature in comparison with that in the blank run using a bare MPS powder is also plotted in the figure. Similarly to the CNZ5 sample, H absorption is weak at RT (L_M ~ 0.03), while η ~ 0.57 eV/H is almost the same as that for the PNZ-type samples discussed above. However, when it is heated up to about 200 °C, significant absorption occurs, and saturate at L_M ~0.8. This behavior is very similar to that observed for the CNZ-type samples.

The CNZ-type samples do not have appreciable amount of the $NiZr_2$ phase, while the $NiZr_2$ phase contributes largely to L_M and η in the PNZ runs. It is inferred that the increase in L_M observed in the #1–2 phases of the CNS-type and the CNZ-type sample is due to reduction of CuO·NiO and Cu·Ni. If we assume that the weak absorption observed in #1-1 RT phases is a result of the Arrhenius law, the activation energy for the reduction can be estimated to be 0.04 eV from the temperature dependence.

In the ET phases of the CNS3 runs, the TC2 temperature is higher than in the control run, giving the excess power, W_{ex}, up to 4.4 W as shown in Fig. 13. In the figure also plotted are the phase-averaged excess heat energy, $\eta_{av,i}$, with the maximum of 5 keV/H, and the integrated excess energy per an absorbent atom, E_a, reaching 200 eV/Ni. The conservatively

defined excess energy, E_{ex}, is 0.9 keV/H at the maximum. These values again suggest nuclear origin of the excess power.

The excess power has been observed also in the H–Cu·Ni system. It is not sufficiently confirmatory, however, since the excess value is only about twice as high as the systematic error of ±2.3 W. It is helpful to mention that the sample CNS2 tested before the start-up of the collaborative research with similar composition to the CNS3 had given much greater excess; W_{ex} ~10 W, $\eta_{av,i}$ ~20 keV/H, E_a ~700 eV/Ni and E_{ex} ~2.0 keV/H [16,17]. It is also valuable and important to note that the CNS3 sample of the same lot was also tested in Tohoku Univ. to obtain W_{ex} ~2–4 W and E_{ex} ~63 eV/H.

S1-type samples

One of the S1-type samples tested is the PS3 sample; Pd nanoparticles supported by the MPS powder. The absorption-heat evolution characteristics in RT phases are similar to the PNZ-type samples. The values of $L_M = 2.1$, $\eta = 0.6$ eV/H and $E_a = 1.2$ eV/Ni in the #1-1 RT phase were all greater than those in the #2-1 RT phase and later, where $L_M = 1.3$, $\eta = 0.20$ eV/H and $E_a = 0.25$ eV/Ni with very good reproducibility.

The value of $L_M = 2.1$, is much smaller than that in the PNZ-type samples, probably due to absence of the $NiZr_2$ phase in this sample. The difference in L_M between #1-1 and #2-1 (and later) is therefore almost solely due to existence/nonexistence of PdO. The η values are smaller than those in the PNZ runs also because of the absence of the $NiZr_2$ phase. In the ET phases, this sample showed no excess power, if we admit the error range of ±2.0 W.

The PSf1 sample is another S1-type sample. It showed very similar, essentially the same, physical quantities both for the RT and the ET phases. The excess power in the ET phases is zero, if we admit the error range of ±2.3 W, as is shown in Fig. 14.

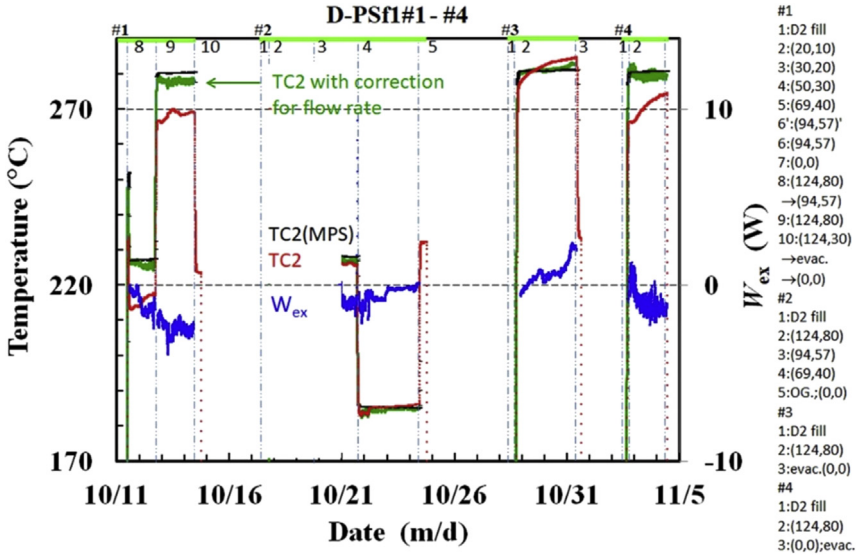

Fig. 14 – Negligible excess power W_{ex} in PSf1 runs at ET.

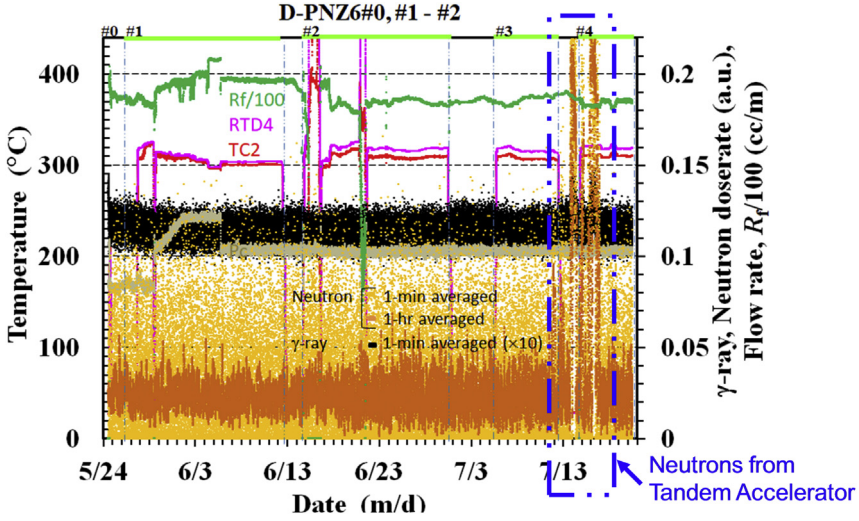

Fig. 15 – Radiations and temperatures at TC2 and RTD4 in PNZ6 runs.

Table 1 – Summary of the results of collaborative experiments (yellow colored) and independently done experiments with PNZt [18], CNZt [18] and CNS2 [16,17]. "M (Ni or Pd) content" is the mass of the majority element, "Pd/Ni or Cu/Ni" is the atomic ratio, "H (D or H)" is the hydrogen isotope introduced into the RC, and "D(H)" means that D_2 gas was mainly used.

Sample ID	M (Ni or Pd) content (g)	Pd/Ni or Cu/Ni	D or H	Room temp. L_M #1	Room temp. L_M #2<	Room temp. $E_t \equiv \int W_a dt$ (kJ/mol-M) #1	Room temp. $E_t \equiv \int W_a dt$ (kJ/mol-M) #2<	Room temp. η_{av} (eV/H) #1	Room temp. η_{av} (eV/H) #2<	Elevated temp. (> 250°C) L_M #1	Elevated temp. L_M #2<	Elevated temp. W_{ex} (W) #1	Elevated temp. W_{ex} (W) #2<	Elevated temp. η_{av} (keV/H) #1	Elevated temp. η_{av} (keV/H) #2<	Elevated temp. $E_{ex} \equiv \int W_a dt / L_M$ (MJ/mol-H) #1	Elevated temp. $E_{ex} \equiv \int W_a dt / L_M$ (MJ/mol-H) #2<
(collab)				#1	#2<	#1	#2<	#1	#2<	#1	#2<	#1	#2<	#1	#2<	#1	#2<
PNZt	6.4	1/7	D(H)	(1.1)	2.2	220	81	(2.1)	0.39	1.5	0.15	5.9	2.6	(0.29)	0.77	(7.8)	4.3
PNZ3	20.0	1/7	D(H)	3.4	1.6	200	62	0.61	0.43	2.8	1.1	8.0	10	6.5	16	3.7	5.7
PNZ3r	18.8	1/7	H	0.11	(5.3)	6.0	0	0.62	0	2.1	(7.4)	8.0	---	0.19	---	2.0	---
PNZ4	23.0	1/7	D	3.5	1.8	180	73	0.56	0.43	3.1	1.1	---	4.5	---	4.4	---	3.0
PNZ5	41.1	1/7	D	3.5	1.1	210	43	0.63	0.4	3.1	0.55	3.5	4.2	0.4	2.7	1.1	7.6
PNZ5r	40.7	1/7	D(H)	0.32	0.085	16	1.4	0.53	0.17	0.7	0.2	4.0	5.5	0.03	23	2.5	9.0
PNZ6	27.2	1/10	D(H)	3.5	1.2	190	48	0.58	0.41	2.8	0.62	24	17	0.35	16	14	44
PNZ6r	25.2	1/10	D	0.8	0.25	39	0.086	0.51	0.34	0.5	0.25	8	10	270	7.5	54	85
PNZ7k	20.8	1/7	D	3.4	1.3	190	49	0.56	0.38	2.6	0.7	4.2	3.1	2.6	1.4	2.5	3.4
CNZt	9.1	1/7	H(D)	0.19	0.19	6.7	3.7	0.37	0.2	1.7	0.2	4.0	2.2	1.7	0.83	11	150
CNZ5	22.0	1/7	H	0.2	===	9.8	===	0.50	===	1.9	===	8.0	===	2.8	===	2.6	===
CNS2	12.1	1/7	H	0.01	===	0	===	0	===	1.1	0.15	11	7.2	11	20	23	190
CNS3	11.4	1/10	H	0.03	0.02	1.5	1.5	0.57	0.65	0.8	0.16	2.4	4.4	1.4	4.7	6.0	90
PS3	17.3	∞	H(D)	2.1	1.3	130	25	0.60	0.20	0.9	0.7	===	< 1.7	0	0	0.0	0
PSf1	8.4	∞	D	2.6	1.6	130	29	0.51	0.19	1.6	0.7	< 1	< 2.2	0	0	0	0

It should be noted that the PSn1 sample tested in Tohoku Univ. also produced no excess heat. From these results, we conclude as one of the important findings that nanocomposites of two or more metal elements are necessary to form the reaction field for induction of AHE producing sustainably weeks-lasting excess heat power at ET.

Ionizing radiations and possible explanation

Finally, ionizing radiation measurements are discussed. An example of the result of measurements of the γ-ray counting rate and the neutron dose rate in the PNZ6 sample is shown in Fig. 15. The γ-ray counting rate and the neutron dose rate are steady with rather large fluctuation, except for a period with high neutron dose rate in middle July. However, the period agrees with the period when the accelerator in the next room was operated in the neutron emitting mode. We conclude that no observable level of hard radiation accompanies the excess heat at least up to the power level observed in the present work.

Another feature of the present AHE is that little isotope effect is distinguishable. The excess power is of the same order of magnitude for the systems with either D-Pd·Ni, H–Pd·Ni or H–Cu·Ni. It might be probable that the reaction producing the excess heat takes place between the hydrogen isotopes, and that the metal lattice only provide a field of the reaction. If we assume a nuclear origin of the excess energy, it might look curious at first glance that the isotope effect is so small. A possible explanation of the phenomena is found in Takahashi theory [20–22].

Summary and concluding remarks

Hydrogen isotope absorption and heat evolution both at RT and ET have been examined for two kinds of ZrO_2-supported Pd·Ni or Cu·Ni nanocomposites and two kinds of SiO_2-supported CuNi nanocomposites and Pd nanoparticles. The results are tabulated in Table 1, and summarized as follows;

(1) Observed absorption L_M and heat evolution η at RT were not anomalously large, and could be of explainable levels by some chemical processes.
(2) At ET of 200–300 °C, most samples with binary metal nanocomposites produced excess power W_{ex} of 3–24 W sustainably lasting for up to several weeks.
(3) The excess power W_{ex} was observed not only in the D-Pd·Ni system but also in the H–Pd·Ni system and H–Cu·Ni system.
(4) On the other hand, single-element nanoparticle samples (PS3 and PSf1) produced no excess heat at ET.
(5) PNZ6 and PNZ6r samples with Pd/Ni = 1/10 generated much higher excess power W_{ex} and exess energies η_{av} and E_{ex} than other PNZ samples with Pd/Ni = 1/7. The Pd/Ni ratio is one of the keys to increase the excess power.
(6) The maximum phase-averaged excess heat energy, $\eta_{av,i}$, recorded with PNZ6r exceeded 270 keV/D (26 GJ/mol-D), and the integrated excess energy E_a reached 1 keV/Pd·Ni (100 MJ/mol-M) and E_{ex} = 90 MJ/mol-H (CNS3).

(7) It is impossible to attribute the excess energy to any chemical reaction; it is possibly due to radiation-free nuclear process.

The anomalous heat effect was observed with very small amount of D(H) transfer in both direction of net absorption and net desorption. It is conceived that this might be a hint for AHE generation sites and some nuclear mechanism in the binary metal nanocomposite samples and may match with the models by Takahashi TSC theories.

The AHE is repeatable in the metal-hydrogen-isotope-gas system at elevated temperature, typically ca. 300 °C, by using Ni-based binary metal nanocomposites with Pd or Cu atoms with minor molar ratio, and continues for a month or more. Key issues to be solved are 1) synthesis method of controlled 2–20 nm size Pd–Ni or Cu–Ni binary-nano-metal islands in supporter zirconia or silica of several-micron-sized flakes, 2) optimum Pd/Ni or Cu/Ni molar ratio to gain larger excess thermal power level and larger energy density released, 3) trials of establishing stimulation fields to enhance the AHE, as well as finding optimum running temperature and gas-pressure.

REFERENCES

[1] Celani F, Marano EF, Ortenzi B, Pella S, Bartalucci S, Micciulla F, et al. Cu-Ni-Mn alloy wires, with improved sub-micrometric surfaces, used as LENR device by new transparent, dissipation-type, calorimeter. J Condensed Matter Nucl Sci 2014;13:56–67.

[2] F. Piantelli/Nichenergy; http://www.nichenergy.com/results.html.

[3] A. Rossi/Leonardo Corporation; http://ecat.com/.

[4] G. Levi, E. Foschi, B. Höistad, R. Pettersson, L. Tegner and H. Essen., http://www.sifferkoll.se/sifferkoll/wp-content/uploads/2014/10/LuganoReportSubmit.pdf.

[5] Parkhomov AG. Int J Unity Sci 2014;6(2):57–61. ibid. 7(3) (2015) 68-72; ibid. 8(3) (2015) 34–39.

[6] S. Jiang, http://ja.scribd.com/doc/267085905/New-Result-on-Anomalous-Heat-Production-in-Hydrogen-loaded-Metals-at-High-Temperature, (2015).

[7] J. Cole, http://www.lenr-coldfusion.com/2015/04/16/experiment-generates-apparent-excess-heat/, (2015).

[8] Takahashi A, Kitamura A, Takahashi K, Seto R, Yokose T, Taniike A, et al. Anomalous heat effects by interaction of nano-metals and d(H)-gas. Tohoku University; 2016. p. 13–25. published in Proc. ICCF20.

[9] Kitamura Akira, Takahashi Akito, Takahashi Koh, Seto Reiko, Matsuda Yuki, Iwamura Yasuhiro, et al. Collaborative examination on anomalous heat effect using nickel-based binary nanocomposites supported by zirconia. J Condensed Matter Nucl Sci 2017;24:202–13 (Proc. ICCF20).

[10] Iwamura Y, Itoh T, Kasagi J, Kitamura A, Takahashi A, Takahashi K. Replication experiments at Tohoku university on anomalous heat generation using nickel-based binary nanocomposites and hydrogen isotope gas. J Condensed Matter Nucl Sci 2017;24:191–202 (Proc. ICCF20).

[11] Kitamura A, Takahashi A, Takahashi K, Seto R, Hatano T, Iwamura Y, et al. Heat evolution from silica-supported nano-composite samples under exposure to hydrogen isotope gas. 2017. p. 1–14. Proc. JCF17 (http://jcfrs.org/file/jcf17-proceedings.pdf).

[12] Iwamura Y, Itoh T, Kasagi J, Kitamura A, Takahashi A, Takahashi K, et al. Anomalous heat generation experiments using metal nanocomposites and hydrogen isotope gas. 2017. p. 15–27. Proc. JCF17 (http://jcfrs.org/file/jcf17-proceedings.pdf).

[13] Kitamura Akira, Takahashi Akito, Takahashi Koh, Seto Reiko, Hatano Takeshi, Iwamura Yasuhiro, et al. "Effect of supporter material on heat evolution from Ni-based nano-composite samples under exposure to hydrogen isotope gas". In: Presented at 12th Int. Workshop on Anomalies in hydrogen-loaded metals, Costigliole d'Asti, Italy; June 2017. p. 5–9.

[14] Iwamura Y, Itoh T, Kasagi J, Kitamura A, Takahashi A, Takahashi K, et al. "Anomalous heat generation experiments using metal nanocomposites and hydrogen isotope gas". In: Presented at 12th Int. Workshop on Anomalies in hydrogen-loaded metals, Costigliole d'Asti, Italy; June 2017. p. 5–9.

[15] Kitamura A, Takahashi A, Seto R, Fujita Y, Taniike A, Furuyama Y. Brief summary of latest experimental results with a mass-flow calorimetry system for anomalous heat effect of nano-composite metals under D(H)-gas charging. Curr Sci 2015;108(4):589–93.

[16] Kitamura A, Takahashi A, Seto R, Fujita Y, Taniike A, Furuyama Y. Comparison of some Ni-based nano-composite samples with respect to excess heat evolution under exposure to hydrogen isotope gases. 2015. p. 1–19. Proc. JCF15 (http://jcfrs.org/file/jcf15-proceedings.pdf).

[17] Kitamura A, Takahashi A, Seto R, Fujita Y, Taniike A, Furuyama Y. Effect of minority atoms of binary Ni-Based nano-composites on anomalous heat evolution under hydrogen absorption. J. Condensed Matter Nucl. Sci 2016;19:135–44 (Proc. ICCF19(2015)).

[18] Kitamura A, Marano EF, Takahashi A, Seto R, Yokose T, Taniike A, et al. Heat evolution from zirconia-supported Ni-based nano-composite samples under exposure to hydrogen isotope gas. 2016. p. 1–16. Proc. JCF16 (http://jcfrs.org/filr/jcf16-proceedings.pdf).

[19] Arata Y, Zhang Y. The special report on research project for creation of new energy. J High Temp Soc 2008;34:85–93.

[20] Takahashi Akito. Physics of cold fusion by TSC theory. J Phys Sci Appl 2013;3:191–8.

[21] Takahashi Akito. Fundamental of rate theory for CMNS. J Condensed Matt Nucl Sci 2016;19:298–315.

[22] Takahashi Akito. Chaotic end-state oscillation of 4H/TSC and WS fusion. 2016. p. 41–65. Proc. JCF-16 (http://jcfrs.org/file/jcf16-proceedings.pdf).